Fluctuation and Noise Letters
Vol. 8, Nos. 3–4 (2008) L369–L379
© World Scientific Publishing Company

World Scientific
www.worldscientific.com

VECTOR FIELD DESIGN OF SCREW-TYPE CHAOS

NEBU JOHN MATHAI, TAKIS ZOURNTOS and DEEPA KUNDUR
Texas A&M University
College Station, TX 77843-3128, USA
mathai@ieee.org, {takis,deepa}@tamu.edu

Communicated by Tamas Kalmar-Nagy

The design of a screw-type chaotic system in $\mathcal{R}^3$ is presented whereby the dynamical equations are constructed using geometric methods that produce a vector field with the desired properties. We utilize piecewise linear and constant dynamics for simplicity; the piecemeal dynamics are combined using switching functions. An analysis of the system shows invariance and the absence of equilibria — implying the existence of limit cycles and strange attractors; a bifurcation diagram confirms the existence of these behavioral modes and that the system undergoes a period-doubling cascade to chaos. We finally present a hardware realization of this system, and oscilloscope traces showing a chaotic system trajectory.

Keywords: Chaos; nonlinear circuits; nonlinear oscillators; nonlinear systems.

1. Introduction

Systems exhibiting complex dynamics such as chaos are finding application in a variety of contexts. For instance, the application of chaos to cryptography is discussed in [1, 2], while [3] considers its application to communications. The use of complex dynamics to enable computation over the real numbers through the embedding of a $\mathcal{R}^2$ discrete dynamical system (which encodes a Turing machine) within a continuous $\mathcal{R}^3$ flow is discussed in [4, 5]. Further, the application of chaotic neural network models in parallel distributed computation is presented in [6]. Hence, there is considerable motivation to study methods of synthesizing dynamical systems with specific properties that are amenable to implementation.

Rössler's work in the 1970s produced some of the earliest studies of chaotic systems in $\mathcal{R}^3$ from the perspective of designing them. In [7], Rössler modifies a dynamical primitive for periodic oscillation to obtain chaos. Specifically, after system trajectories rotate out of a region of state space (e.g., due to an unstable focus), they are reintroduced (reinjected) back into the rotational region; the result is a dynamical system whose flow embeds Smale's horseshoe map — leading to

chaos [8]. Beyond this, [9] presented several additional prototypes of chaotic motion, including a mode Rössler termed "screw-type" chaos.

A survey of the literature yields a large body of more recent work pertaining to the engineering of chaotic systems, of which a sample can be found in [10–18]. The focus of these works include extending the types of attractor structures that could be designed (e.g., multi-scroll and multi-screw attractors), exploring nonlinearities that are more amenable to implementation (e.g., piecewise linear, piecewise constant, and switching functions), electronic circuit implementation perspectives, and the development of design and analytical techniques for chaotic systems.

Methods that use piecewise-linear or piecewise-constant dynamics to realize nonlinear systems are of particular interest due to the potential for economical implementation. Not only are the linear and constant "pieces" straightforward to realize, but they can also be easily "stitched" together via switching and Boolean circuits to construct the overall system. Moreover the simplified linear and constant dynamics (leading to trajectories in state space that are exponential and linear, respectively) makes these systems conducive to analysis (e.g., enabling the derivation of explicit return maps) [14].

1.1. *Contributions and outline of the paper*

In this work we consider the development of a novel screw-type chaotic attractor from a geometric perspective where the equations of motion are formed by constructing a vector field to realize the desired behavior. We address a realization for screw-type chaos due to the relatively sparse treatment of circuit implementations for screw-type chaos in the literature. Piecewise linear and constant dynamics are used to implement the vector field in piecemeal fashion; Boolean functions are used to stitch the pieces together to form the overall system. Section 2 explains the design of our system, while section 3 presents some properties of the system such as invariance and bifurcation phenomenon (including the emergence of chaos). Section 4 presents our circuit realization and an oscilloscope trace from our implementation. We conclude with some remarks on future work.

2. Vector Field Design of the Proposed System

2.1. *Vector field design*

Given the dynamical system $\dot{\mathbf{x}} = \mathbf{f}(\mathbf{x})$, $\mathbf{x} := (x_1, x_2, x_3) \in \mathcal{R}^3$, the right-hand side $\mathbf{f} : \mathcal{R}^3 \to \mathcal{R}^3$ defines a vector field over $\mathcal{R}^3$ such that at each state, $\mathbf{x}$, the system evolves according to the instantaneous velocity given by $\mathbf{f}(\mathbf{x})$. In this work we design our system by first identifying the structure of the desired flow through state space, from which the qualitative geometry of the vector field we wish to realize can be obtained. We then develop a corresponding map that yields a vector field with this geometric structure.

2.2. *Screw-type chaos*

In Rössler's studies of chaotic dynamics, a suite of systems, each exhibiting different prototypical chaotic modes were developed [9], including screw-type chaos. With screw-type chaos, trajectories rotate along a quasi-cylindrical region (the "screw" from which this mode of chaos derives its name [19]) of $\mathcal{R}^3$ until they exit from one

end–the "top"–of the cylinder and reinject back into the "bottom" of the cylinder. Figure 1 illustrates the structure of a vector field over $\mathcal{R}^3$ that yields a screw type flow. The screw occupies the subsets labeled $\mathbf{S}_+$ and $\mathbf{S}_-$, while the reinjection takes place through the subsets $\mathbf{H}_1$, $\mathbf{H}_2$ and $\mathbf{H}_3$. A typical system trajectory, Γ, is indicated on the figure.

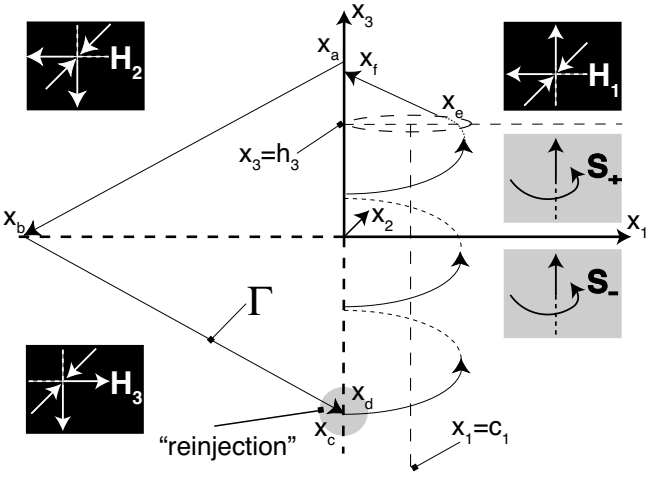

Fig. 1. Vector field structure of the proposed system. Horizontal vectors specify the x_1 component of motion, slanted vectors show the x_2 component perpendicular to the page, and vertical vectors show the x_3 component. The curved vectors indicate rotation parallel to the $x_1 - x_2$ plane. Note: the $x_2 > 0$ region is *behind* the plane of the page.

2.3. *Vector field design of screw-type chaos*

Figure 1 illustrates the structure of a screw-type flow. The overall motion can be divided into two submodes, rotation and reinjection, suggesting a piecewise construction of the corresponding vector field, $\mathbf{f} : \mathcal{R}^3 \to \mathcal{R}^3$. Accordingly, we partition the state space into disjoint, connected subsets, $\mathbf{S} := \mathbf{S}_- \cup \mathbf{S}_+$ (the screw, within which rotation occurs) and $\mathbf{H} := \mathbf{H}_1 \cup \mathbf{H}_2 \cup \mathbf{H}_3$ (within which reinjection occurs) where:

$$\begin{aligned}
\mathbf{S}_- &= \{\mathbf{x} : x_1 \geq 0, x_3 < 0\} \\
\mathbf{S}_+ &= \{\mathbf{x} : x_1 \geq 0, 0 \leq x_3 \leq h_3\} \\
\mathbf{H}_1 &= \{\mathbf{x} : x_1 \geq 0, x_3 > h_3\} \\
\mathbf{H}_2 &= \{\mathbf{x} : x_1 < 0, x_3 \geq 0\} \\
\mathbf{H}_3 &= \{\mathbf{x} : x_1 < 0, x_3 < 0\}
\end{aligned}$$

In Fig. 1, the black-on-grey and white-on-black labels denote various partitions of $\mathcal{R}^3$ and the associated vector fields therein.

Within $\mathbf{S}$, the dynamics in the $x_1 - x_2$ plane are decoupled from the dynamics along the x_3 axis and are those of a system oscillating sinusoidally about $\mathbf{G} := \{\mathbf{x} \in$

$\mathbf{S} : x_1 = c_1, x_2 = 0\}$. The dynamics in the x_3 direction within $\mathbf{S}$ is constant and positive, bringing the flow upwards towards $\mathbf{H}_1$. This is shown on the black-on-grey labels in the figure. The following dynamical equations implement this behavior:

$$\begin{aligned} \dot{x}_1 &= -\omega x_2 \\ \dot{x}_2 &= \omega(x_1 - c_1) \\ \dot{x}_3 &= +v_3 \end{aligned} \tag{1}$$

where ω sets the frequency of the $x_1 - x_2$ sinusoidal oscillator, c_1 sets the bias of the oscillator in the x_1 direction, and v_3 sets the speed of system trajectories in the x_3 direction.

The dynamics in $\mathbf{H}$ have a dual purpose:

- contracting the flow in the x_2 direction
- reinjecting the flow from the top of $\mathbf{S}$ back into the bottom of $\mathbf{S}$

Flow contraction is achieved by setting the x_2 dynamics to asymptotically stabilize the $x_2 = 0$ plane (i.e., setting $\dot{x_2} = -k_2 x_2$). To achieve reinjection, we design the system using piecewise-constant dynamics to steer the flow and take trajectories out of the "top" of $\mathbf{S}_+$ at $x_3 = h_3$ through $\mathbf{H}_1$, $\mathbf{H}_2$, $\mathbf{H}_3$, and back into $\mathbf{S}_-$. In $\mathbf{H}_1$ we allow the flow to continue in the $+x_3$ direction while switching the x_1 dynamics to flow in the $-x_1$ direction, bringing the system to $\mathbf{H}_2$. Within $\mathbf{H}_2$, the x_1 motion remains unchanged while the x_3 motion switches to the $-x_3$ direction. Arriving at $\mathbf{H}_3$, the system maintains its x_3 motion while switching the x_1 component to flow in the $+x_1$ direction — towards the $x_3 < 0$ part of $\mathbf{S}$. This behavior is implemented by the following dynamical equations:

$$\begin{aligned} \dot{x}_1 &= \begin{cases} +v_1, & \mathbf{x} \in \mathbf{H}_3 \\ -v_1, & \mathbf{x} \in \mathbf{H}_1 \cup \mathbf{H}_2 \end{cases} \\ \dot{x}_2 &= -k_2 x_2 \\ \dot{x}_3 &= \begin{cases} +v_3, & x_1 \geq 0 \\ -v_3, & x_1 < 0 \end{cases} \end{aligned} \tag{2}$$

where v_1 and v_3 set the speed of trajectories in the x_1 and x_3 directions.

We can now combine the separate pieces of $\mathbf{f}$ defined above in (1) and (2) to compose the overall dynamical system:

$$\begin{aligned} \dot{x}_1 &= \begin{cases} +v_1, & \mathbf{x} \in \mathbf{H}_3 \\ -v_1, & \mathbf{x} \in \mathbf{H}_1 \cup \mathbf{H}_2 \\ -\omega x_2, & \mathbf{x} \in \mathbf{S} \end{cases} \\ \dot{x}_2 &= \begin{cases} \omega(x_1 - c_1), & \mathbf{x} \in \mathbf{S} \\ -k_2 x_2, & \mathbf{x} \in \mathbf{H} \end{cases} \\ \dot{x}_3 &= \begin{cases} +v_3, & x_1 \geq 0 \\ -v_3, & x_1 < 0 \end{cases} \end{aligned} \tag{3}$$

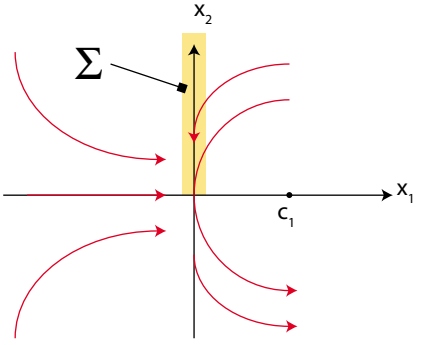

Fig. 2. Illustration of the vector field that gives rise to a sliding mode along the plane $\mathbf{\Sigma}$ (note: $x_3 < 0$).

3. Properties

3.1. *Analysis*

Lemma 3.1 (Subspace Transition Order)**.** *System (3) never remains in any one subset indefinitely; transitions between subsets occur according to the following mechanism:*

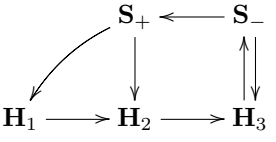

Proof. We have $\mathbf{f}(\mathbf{x}) \neq \mathbf{0}, \forall \mathbf{x} \in \mathcal{R}^3$, precluding the existence of equilibria. As well, the linear and constant dynamics that govern the system do not exhibit finite escape times. In $\mathbf{H}$, the result follows directly from the solution of (3) in $\mathbf{H}$:

$$\mathbf{x}(t) = \begin{pmatrix} x_1(t) \\ x_2(t) \\ x_3(t) \end{pmatrix} = \begin{pmatrix} x_1(t_e) - v_1(t - t_e)\mathrm{sgn}(x_3(t)) \\ x_2(t_e)e^{-k_2(t-t_e)} \\ x_3(t_e) + v_3(t - t_e)\mathrm{sgn}(x_1(t)) \end{pmatrix}$$

where the system enters subset $\mathbf{H}_e$ at time t_e (for $e \in \{1, 2, 3\}$), and $x_i(t_e)$ denotes the coordinate of the ith state at time t_e (for $i \in \{1, 2, 3\}$). In $\mathbf{S}_-$, the system can move to $\mathbf{H}_3$ since $\dot{x}_1 < 0$ on the interface $x_1 = 0$ for $x_2 > 0$; otherwise, the solution $x_3(t) = x_3(t_e) + v_3(t - t_e)$ ensures the system will reach $\mathbf{S}_+$ in finite time. Finally, in $\mathbf{S}_+$ the system can move to $\mathbf{H}_2$ since $\dot{x}_1 < 0$ on the interface $x_1 = 0$ for $x_2 > 0$; otherwise, the solution $x_3(t) = x_3(t_e) + v_3(t - t_e)$ ensures the system will reach $\mathbf{H}_1$ in finite time. □

The existence of a sliding mode. We note the existence of a sliding mode (indicated above by $\mathbf{H}_3 \rightleftarrows \mathbf{S}_-$) along the plane $\mathbf{\Sigma} := \{\mathbf{x} : x_1 = 0, x_2 > 0, x_3 < 0\}$ between $\mathbf{H}_3$ and $\mathbf{S}_-$ in which the x_1 component of the vector field on both sides of $\mathbf{\Sigma}$ point towards it. Figure 2 illustrates the vector field that points towards

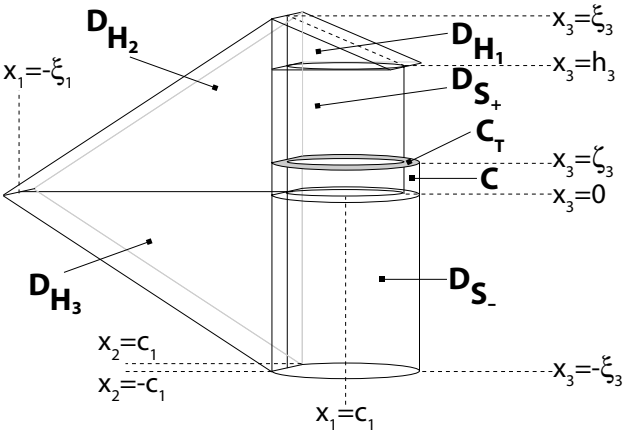

Fig. 3. Structure of the bounding region $\mathbf{D}$.

$\mathbf{\Sigma}$; as the figure indicates, and the equations of motion specify, on $\mathbf{\Sigma}$, $\dot{x_2} = -\omega c_1$ (setting $x_1 = 0$ in (3)), and hence will bring the x_2 component of trajectories on $\mathbf{\Sigma}$ to $x_2 = 0$ in finite time. Hence trajectories sliding along $\mathbf{\Sigma}$ will reach the line $\mathbf{L} := \{\mathbf{x} : x_1 = 0, x_2 = 0\} \nsubseteq \mathbf{\Sigma}$ in finite time, thus exiting the sliding mode. Trajectories which reach $\mathbf{L}$ satisfy $(x_1 - c_1)^2 + x_2^2 = c_1^2$ and hence will only return to the plane $\{\mathbf{x} \in \mathbf{S} : x_1 = 0\}$ when $x_2 = 0$ (i.e., they will not[1] hit $\mathbf{\Sigma}$ again, nor will they exit to $\mathbf{H}_2$ from $\mathbf{S}_+$).

Definition 3.1. Consider the regions of $\mathcal{R}^3$ illustrated in Figure 3; for $\mathbf{x} = (x_1, x_2, x_3) \in \mathcal{R}^3$, we define:

$$
\begin{aligned}
\mathbf{D}_{\mathbf{H}_1} &= \{\mathbf{x} : 0 \le x_1 \le \xi_2, |x_2| \le c_1, h_3 < x_3 \le -\frac{v_3}{v_1}x_1 + \xi_3\} \\
\mathbf{D}_{\mathbf{H}_2} &= \{\mathbf{x} : -\xi_1 \le x_1 < 0, |x_2| \le c_1, 0 \le x_3 \le +\frac{v_3}{v_1}x_1 + \xi_3\} \\
\mathbf{D}_{\mathbf{H}_3} &= \{\mathbf{x} : -\xi_1 \le x_1 < 0, |x_2| \le c_1, -\frac{v_3}{v_1}x_1 - \xi_3 \le x_3 < 0\} \\
\mathbf{D}_{\mathbf{S}_+} &= \{\mathbf{x} : (x_1 - c_1)^2 + x_2^2 \le c_1^2, 0 \le x_3 \le h_3\} \\
\mathbf{D}_{\mathbf{S}_-} &= \{\mathbf{x} : x_1 \ge 0, (x_1 - c_1)^2 + x_2^2 \le 2c_1^2, -\xi_3 \le x_3 < 0\} \\
\mathbf{D} &= \mathbf{D}_{\mathbf{H}_1} \cup \mathbf{D}_{\mathbf{H}_2} \cup \mathbf{D}_{\mathbf{H}_3} \cup \mathbf{D}_{\mathbf{S}_+} \cup \mathbf{D}_{\mathbf{S}_-} \\
\mathbf{C} &= \{\mathbf{x} : x_1 \ge 0, (x_1 - c_1)^2 + x_2^2 \le 2c_1^2, 0 \le x_3 \le \zeta_3\} \\
\mathbf{C}_T &= \{\mathbf{x} : x_1 \ge 0, (x_1 - c_1)^2 + x_2^2 \le 2c_1^2, x_3 = \zeta_3\} \subset \mathbf{C}
\end{aligned}
$$

where:

$$
\xi_1 = \frac{v_1}{v_3}h_3 + \xi_2, \quad \xi_2 = 2c_1, \quad \xi_3 = h_3 + \frac{v_3}{v_1}\xi_2, \quad \zeta_3 = \frac{2\pi v_3}{\omega}
$$

[1]We note, however, that in the case of systems realized physically (as opposed to systems simulated via numerical integration where tests for equality can be done accurately), effects such as non-ideal switching may cause these transitions to occur.

Further, we denote the *surface* of $\mathbf{D} \cup \mathbf{C}$ by surf($\mathbf{D} \cup \mathbf{C}$).

Lemma 3.2 (Surface Vector Field)**.** *Let* $\mathbf{n}_l(\mathbf{x})$ *denotes the family of vectors (parameterized by* $l > 0$*) normal to surf*$(\mathbf{D} \cup \mathbf{C}) - \mathbf{C}_T$ *at* $\mathbf{x}$*. Then*:

$$p_l(\mathbf{x}) = \mathbf{n}_l(\mathbf{x}) \cdot \mathbf{f}(\mathbf{x}) \leq 0, \quad \forall \mathbf{x} \in \textit{surf}(\mathbf{D} \cup \mathbf{C}) - \mathbf{C}_T$$

Proof. On the curved surfaces of $\mathbf{D}_{\mathbf{S}_-}$, $\mathbf{D}_{\mathbf{S}_+}$ and $\mathbf{C}$:

$$p_l(\mathbf{x}) = l \begin{pmatrix} x_1 - c_1 \\ x_2 \\ 0 \end{pmatrix} \cdot \begin{pmatrix} -\omega x_2 \\ \omega(x_1 - c_1) \\ v_3 \end{pmatrix} = 0$$

while on the $x_3 = -\xi_3$ face of $\mathbf{D}_{\mathbf{S}_-}$:

$$p_l(\mathbf{x}) = l \begin{pmatrix} 0 \\ 0 \\ -1 \end{pmatrix} \cdot \begin{pmatrix} -\omega x_2 \\ \omega(x_1 - c_1) \\ v_3 \end{pmatrix} = -l v_3 < 0$$

On the $|x_2| = \pm c_1$ planes bounding $\mathbf{D}_{\mathbf{H}_1}$, $\mathbf{D}_{\mathbf{H}_2}$ and $\mathbf{D}_{\mathbf{H}_3}$:

$$p_l(\mathbf{x}) = l \begin{pmatrix} 0 \\ \text{sgn}(x_2) \\ 0 \end{pmatrix} \cdot \begin{pmatrix} \pm v_1 \\ -k_2 x_2 \\ \pm v_3 \end{pmatrix} = -l k_2 |x_2| < 0$$

while on the slanted planes:

$$p_l(\mathbf{x}) = l \begin{pmatrix} v_3 \text{sgn}(x_1) \\ 0 \\ v_1 \text{sgn}(x_3) \end{pmatrix} \cdot \begin{pmatrix} -v_1 \text{sgn}(x_3) \\ -k_2 x_2 \\ v_3 \text{sgn}(x_1) \end{pmatrix} = 0$$

and on the $x_3 = h_3$ face of $\mathbf{D}_{\mathbf{H}_1}$:

$$p_l(\mathbf{x}) = l \begin{pmatrix} 0 \\ 0 \\ -1 \end{pmatrix} \cdot \begin{pmatrix} -v_1 \\ -k_2 x_2 \\ v_3 \end{pmatrix} = -l v_3 < 0$$

□

Theorem 3.1 (Invariance)**.** *Let* $h_3 > \zeta_3$*. For any state in* $\mathbf{D}$*, the system will forever remain within* $\mathbf{D} \cup \mathbf{C}$*.*

Proof. By Lemma 3.2, no trajectory started in $\mathbf{D} \subset \mathbf{D} \cup \mathbf{C}$ can leave through surf($\mathbf{D} \cup \mathbf{C}$) $- \mathbf{C}_T$ since the vector field never points out of this surface. Thus, the only mechanism for escape is through the unaccounted surface, $\mathbf{C}_T$.

By Lemma 3.1, solutions entering $\mathbf{C}$ must enter from $\mathbf{D}_{\mathbf{S}_-}$ at $x_3 = 0$ and satisfy $(x_1 - c_1)^2 + x_2^2 \leq 2c_1^2$. The dynamics in the $x_1 - x_2$ plane in $\mathbf{S}$ causes trajectories to rotate about $\mathbf{G}$ with period $\frac{2\pi}{\omega}$. For $(x_1 - c_1)^2 - x_2^2 \leq c_1^2$, the system will remain in $\mathbf{D}_{\mathbf{S}_+}$, by definition. Otherwise, if $c_1^2 < (x_1 - c_1)^2 - x_2^2 \leq 2c_1^2$, the system will enter $x_1 = 0$ with $0 < x_2 \leq c_1$ *prior* to executing a full rotation (i.e., $\Delta t < \frac{2\pi}{\omega}$); since, in this region, $\dot{x_1} < 0$ and $|x_2| \leq c_1$, the system will then move to $\mathbf{D}_{\mathbf{H}_2}$, by definition. As $\dot{x_3} = v_3$ and $\Delta t < \frac{2\pi}{\omega}$, this exit from $\mathbf{C}$ to $\mathbf{D}_{\mathbf{H}_2}$ occurs at $x_3 < \frac{2\pi v_3}{\omega} = \zeta_3$ which is strictly *below* $\mathbf{C}_T$. □

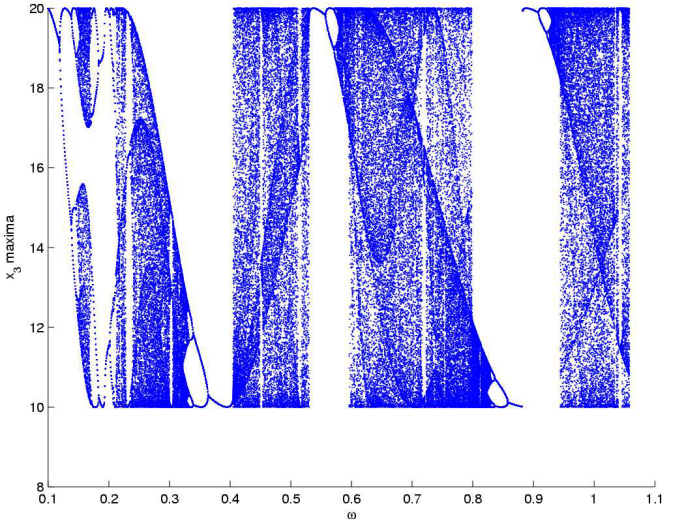

Fig. 4. Bifurcation diagram for the system with parameters $(v_1, v_3, c_1, h_3, k_2) = (1, 1, 5, 10, 1)$ and initial state $(0.1, 0.1, 0.1)$; the ω axis has a step size of 0.0005. The simulation was run for 4000 s and the local maxima of x_3 were plotted on the vertical axis (the first half of the set of maxima were discarded to remove transients).

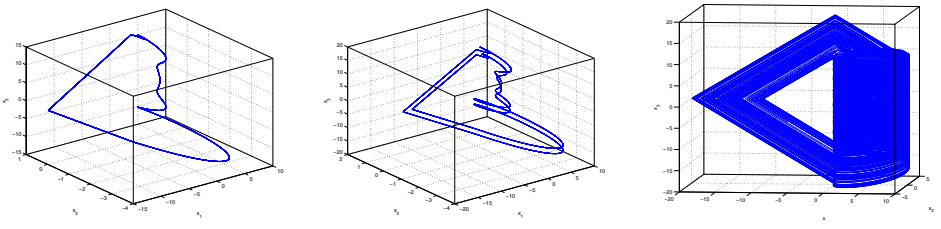

(a) Period-one cycle ($\omega = 0.7$) (b) Period-two cycle ($\omega = 0.55$) (c) Chaotic ($\omega = 1$)

Fig. 5. Behavioral modes.

3.2. *Bifurcation diagram and behavioral modes*

The results of the previous section indicate that under appropriate conditions the system stays confined to a bounded region of state space. In $\mathcal{R}^3$, this implies the existence of stable limit cycles, strange attractors or quasiperiodic trajectories (equilibria being precluded by Lemma 3.1). To investigate the change in system behavior as ω is varied, we generated the bifurcation diagram of Fig. 4. We see that as ω is varied, the system undergoes a period-doubling cascade into chaos [20]. That chaos should manifest itself is not surprising since various features of chaotic systems are present including the reinjection of flows that have been rotated [9] and dissipation (controlled by k_2). Three behavioral modes are shown in Figs. 5(a)-5(c).

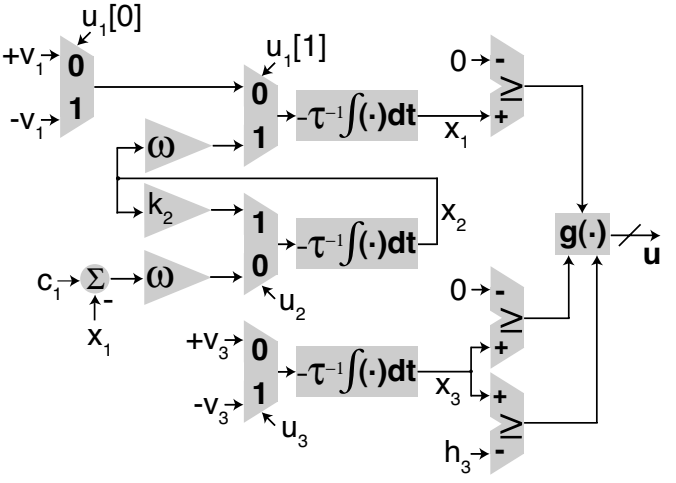

Fig. 6. Hardware topology for the proposed chaotic system.

4. Implementation

Figure 6 illustrates the architecture of our circuit realization, where the Boolean function, $\mathbf{g}(\mathbf{x})$, is defined as:

$$\begin{aligned} u_1[0] =& (x_1 < 0) \cap (x_3 < 0) \\ u_1[1] =& \neg(u_1[0]) \cap \\ & \neg\{(x_3 > h_3) \cup [(x_3 \geq 0) \cap (x_1 < 0)]\} \\ u_2 =& (x_1 \geq 0) \cap (x_3 \leq h_3) \\ u_3 =& x_1 \geq 0 \end{aligned}$$

and $\neg$, $\cap$, and $\cup$ represent logical NOT, AND, and OR, respectively.

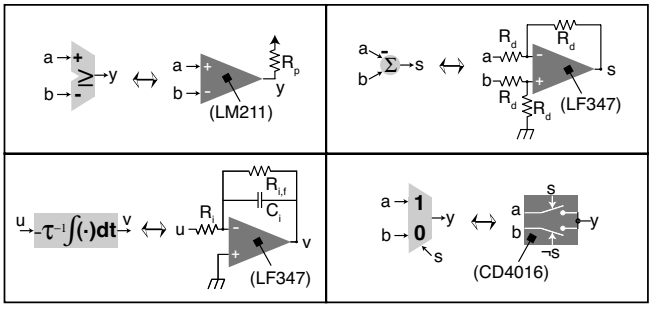

Fig. 7. Circuits used to realize the architecture.

Using the circuits of Fig. 7, the system was constructed. Figure 8(b) shows an oscilloscope trace for the projection of a chaotic system trajectory on the $x_1 - x_3$ plane.

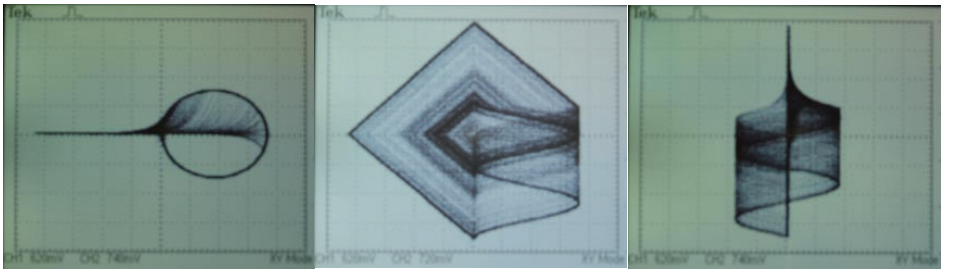

(a) $x_1 - x_2$ projection (b) $x_1 - x_3$ projection (c) $x_2 - x_3$ projection

Fig. 8. Oscilloscope traces.

5. Conclusion

We presented the vector field design of a novel dynamical system that exhibits screw-type chaos. The behavior of the system is confirmed via numerical simulations and experimental results from an electronic circuit realization. Future work will extend the approach to the design of more general structures such as multi-screw and multi-scroll attractors.

References

[1] G. Jakimoski and L. Kocarev, Chaos and cryptography: Block encryption ciphers based on chaotic maps, *IEEE Transactions on Circuits and Systems — Part I: Fundamental Theory and Applications* **48**(2) (2001) 163–169.

[2] F. Dachselt and W. Schwarz, Chaos and cryptography, *IEEE Transactions on Circuits and Systems — Part I: Fundamental Theory and Applications* **48**(12) (2001) 1498–1509.

[3] A. Abel and W. Schwarz, Chaos communications — Principles, schemes, and system analysis, *Proceedings of the IEEE*, Vol. 90, No. 5 (2002), pp. 691–710.

[4] C. Moore, Generalized shifts: unpredictability and undecidability in dynamical systems, *Nonlinearity* **4** (1991) 199–230.

[5] Y. Sato and T. Ikegami, Nonlinear computation with switching map systems, *Journal of Universal Computer Science* **6**(9) (2000) 881–905.

[6] K. Aihara, Chaos engineering and its application to parallel distributed processing with chaotic neural networks, *Proceedings of the IEEE*, Vol. 90, No. 5 (2002), pp. 919–930.

[7] O. E. Rössler, Chaotic behavior in simple reaction systems, *Z. Naturforsch* **31a** (1976) 259–264.

[8] J. Guckenheimer and P. Holmes, *Nonlinear Oscillations, Dynamical Systems, and Bifurcations of Vector Fields*, Springer-Verlag, New York (1983).

[9] O. E. Rössler, Chaos in Abstract Kinetics: Two Prototypes, *Bulletin of Mathematical Biology* **39** (1977) 275–289.

[10] L. O. Chua, M. Komuro, and T. Matsumoto, The Double Scroll Family, *IEEE Transactions on Circuits and Systems* **33** (1986) 1073–1118.

[11] T. Saito, A Chaos Generator Based on a Quasi-Harmonic Oscillator, *IEEE Transactions on Circuits and Systems* **2**(4) (1985) 320–331.

[12] ——, An Approach Toward Higher Dimensional Hysteresis Chaos Generators, *IEEE Transactions on Circuits and Systems* **37**(3) (1990) 399–409.

[13] T. Tsubone and T. Saito, Hyperchaos from a 4-D Manifold Piecewise-Linear System, *IEEE Transactions on Circuits and Systems—Part I: Fundamental Theory and Applications* **45**(9) (1998) 889–894.

[14] ——, Manifold Piecewise Constant Systems and Chaos, *IEICE Trans. Fundamentals* **E82-A**(8) (1999) 1619–1626.

[15] M. Kataoka and T. Saito, A Two-Port VCCS Chaotic Oscillator and Quad Screw Attractor, *IEEE Transactions on Circuits and Systems — Part I: Fundamental Theory and Applications* **48**(2) (2001) 221–225.

[16] Y. Matsuoka and T. Saito, Rich Superstable Phenomena in a Piecewise Constant Nonautonomous Cirucit with Impulsive Switching, *IEICE Trans. Fundamentals* **89-A**(10) (2006) 2767–2774.

[17] T. Matsumoto, Chaos in Electronic Circuits, *Proceedings of the IEEE*, Vol. 75, No. 8 (1987) pp. 1033–1057.

[18] J. Lü, X. Yu, and G. Chen, Generating Chaotic Attractors With Multiple Merged Basins of Attraction: A Switching Piecewise-Linear Control Approach, *IEEE Transactions on Circuits and Systems — Part I: Fundamental Theory and Applications* **50**(2) (2003) 198–207.

[19] C. Letellier, E. Roulin and O. Rössler, Inequivalent topologies of chaos in simple equations, *Chaos, Solitons and Fractals* **28** (2006) 337–360.

[20] K. T. Alligood, T. D. Sauer, and J. A. Yorke, *Chaos: An Introduction to Dynamical Systems*, Springer-Verlag, New York (1996).